Chemical Geology 363 (2014) 40–55

Contents lists available at ScienceDirect

Chemical Geology

journal homepage: www.elsevier.com/locate/chemgeo

Metal release from limestones at high partial-pressures of CO_2

Assaf Wunsch [a,b,*], Alexis K. Navarre-Sitchler [b,e], Joel Moore [c,d], John E. McCray [a,b]

[a] Civil and Environmental Engineering Department, Colorado School of Mines, 1500 Illinois St., Golden, CO 80401, USA
[b] Hydrologic Science and Engineering Program, Colorado School of Mines, 1500 Illinois St., Golden, CO 80401, USA
[c] Department of Physics, Astronomy and Geosciences, Towson University, 8000 York Road, Towson, MD 21252, USA
[d] Urban Environmental Biogeochemistry Laboratory, Towson University, 8000 York Road, Towson, MD 21252, USA
[e] Geology and Geological Engineering Department, Colorado School of Mines, 1500 Illinois St., Golden, CO 80401, USA

ARTICLE INFO

Article history:
Received 6 December 2012
Received in revised form 25 October 2013
Accepted 28 October 2013
Available online 6 November 2013

Editor: J. Fein

Keywords:
Carbon sequestration
Carbonate aquifers
Carbon dioxide leakage
Geochemical modeling
Pressurized experiments

ABSTRACT

CO_2 leakage from underground CO_2 sequestration and storage poses potential risks to degradation of water quality in shallow aquifers. Increased CO_2 concentrations can result in decreased pH and lead to subsequent metal release from mineral dissolution or desorption from mineral surfaces. Dissolution of carbonate minerals present in aquifer sediments or rocks will buffer pH and is generally thought to reduce the potential risk of metal release in the event of a CO_2 leak. As a result, much of the research on geochemical impacts of CO_2 leakage has focused on siliciclastic aquifers with little to no carbonate minerals present. However, carbonate minerals contain trace amounts of metals in their crystal structure that will be released into solution with dissolution and may pose a risk to drinking water quality. Here, we perform laboratory water–rock experiments to analyze the potential for metal release due to carbonate mineral dissolution in limestone aquifers. Rock samples from three limestone aquifers were dissolved in batch reactors with varying partial-pressures of CO_2 (from 0.01 to 1 bar) in the headspace. As CO_2 dissolved into the fluid and decreased the pH, the carbonate minerals dissolved and released metals into solution. The concentrations of calcium, magnesium, strontium, barium, thallium, uranium, and cobalt increased but remained below any regulatory limits. The concentrations of arsenic and nickel increased and exceeded primary drinking water standards set by the USEPA and the State of California, respectively. Potential sources of metals in the rocks were determined through detailed sample characterization using sequential extractions, laser ablation inductively coupled mass spectrometry, and high resolution mineralogical mapping with QEMSCAN. We found that calcite dissolution released more metals to solution than pyrite dissolution or metal desorption from mineral surfaces in these experiments. Geochemical models based on the experimental data were used to evaluate the relative importance of calcite dissolution versus pyrite dissolution over a 30-year time frame. Under both oxic and sub-oxic conditions, calcite dissolution is the dominant source of metals to solution immediately after exposure to CO_2. Pyrite dissolution becomes the dominant source at later times as the fluid reaches equilibrium with respect to calcite. For all model scenarios, the cumulative contribution of metals to solution was dominated by calcite dissolution. Results from this study suggest that the pH-buffering benefit of carbonate mineral dissolution in the event of a CO_2 leak may be offset by the potentially negative effect of trace metal release from the crystal structure. This study highlights the need for detailed sample characterization at individual sites to identify sources of metals when assessing the potential risk of CO_2 leakage into shallow aquifers.

1. Introduction

The increase in global atmospheric CO_2 concentrations has prompted investigations of mitigation actions, including injection of CO_2 into deep geological formations (often referred to as geological carbon-dioxide capture, utilization and sequestration — CCUS). For CCUS to be effective, large amounts of CO_2 need to be captured, compressed, and injected underground. As a compressed supercritical fluid, under geological storage conditions, CO_2 is less dense than surrounding formation waters causing buoyancy-driven upward migration. Suitable injection sites have a good geological seal (caprock), or several seals, which are expected to contain the CO_2 in the intended injection formation (Gaus et al., 2005; Birkholzer et al., 2009; Heath et al., 2011). However, concerns remain about CO_2 leakage through pathways including wells, faults and fractures, driven by large pressure increases in the injection formation (Lindeberg, 1997; Gasda et al., 2004; Duguid and Scherer, 2010).

CO_2 leakage may cause deleterious effects to water quality in freshwater aquifers that overlie injection formations (Harvey et al., 2013).

* Corresponding author at: Civil and Environmental Engineering Department, Colorado School of Mines, 1500 Illinois St., Golden, CO 80401, USA. Tel.: +1 720 290 5133; fax: +1 303 273 3413.
E-mail address: assafwunsch@gmail.com (A. Wunsch).

0009-2541/$ – see front matter © 2013 Elsevier B.V. All rights reserved.
http://dx.doi.org/10.1016/j.chemgeo.2013.10.036

For example, leaking CO_2 can induce geochemical reactions that increase concentrations of unwanted solutes, such as metals (Wang and Jaffe, 2004; Zheng et al., 2009; Apps et al., 2010; Little and Jackson, 2010; Lu et al., 2010; Wilkin and DiGiulio, 2010; Bearup et al., 2012; Frye et al., 2012; Siirila et al., 2012; Atchley et al., 2013; Cahill et al., 2013; Navarre-Sitchler et al., 2013; Wunsch et al., 2013). The increased acidity of CO_2-rich waters is considered the main driver of metal desorption and dissolution of minerals that may contain metals (Wang and Jaffe, 2004; Zheng et al., 2009; Lu et al., 2010). Human health risk associated with increases in metal concentrations in shallow aquifers is an important aspect of risk assessment of CO_2 sequestration projects (Siirila et al., 2012).

To date, little attention has been given to carbonate aquifers in the CO_2-leakage risk-assessment framework. High water transmissivity of carbonate aquifers makes them convenient and important water sources. Globally, an estimated 20–25% of the world's population uses carbonate aquifers for water supply (Ford and Williams, 2007). In the US, carbonate aquifers provide approximately 17% of the groundwater supply used for public consumption (Maupin and Barber, 2005), and carbonate rocks cover 17% of the land surface (Davies et al., 1984). Carbonate aquifers in the US have high water quality, and generally meet drinking-water standards (Lindsey et al., 2009). Given the ability of carbonate minerals to buffer pH in the event of a CO_2 leak, it has generally been assumed that carbonate aquifers are less likely to be negatively impacted by CO_2 leakage. However, dissolution of carbonate minerals, such as calcite ($CaCO_3$) or dolomite ($CaMg(CO_3)_2$), can release trace metals contained in the crystal lattice (Thorstenson and Plummer, 1977). Many minor and trace elements adsorb to the growing carbonate lattice and get incorporated into the mineral (Comans and Middelburg, 1987; Rouff et al., 2004; Ahmed et al., 2008). Adsorption and subsequent co-precipitation are known to be important metal removing processes in marine environments (Zachara et al., 1991). Divalent cations, such as Mg^{2+}, Mn^{2+}, Co^{2+}, Zn^{2+}, Sr^{2+}, Ba^{2+}, Ni^{2+}, Pb^{2+}, Sc^{2+} and Cd^{2+} can substitute for Ca in the lattice (Zachara et al., 1991; Pingitore et al., 1992; Reeder et al., 1999; Fisler et al., 2000; Harstad and Stipp, 2007). Trivalent cations such as Sc^{3+} (Bogoch et al., 1984), tetravalent ions such as U^{4+} (Sturchio et al., 1998), rare-earth elements (REE) such as Dy^{3+}, Sm^{3+} and Yb^{3+} (Elzinga et al., 2002), structurally-compatible anions such as SeO_4^{2-} (Aurelio et al., 2010), and structurally-incompatible anions such as SO_4^{2-}, BaO_4^{2-}, CrO_4^{2-}, BO_3^{3-} and AsO_3^{3-} (arsenite) and AsO_4^{3-} (arsenate) (Reeder et al., 1994; Alexandratos et al., 2007; Tang et al., 2007; Bardelli et al., 2011) are all potentially found at trace concentrations in calcite.

Despite the evidence of metal association, carbonate minerals are not perceived as metal sources in most CCUS-modeling works, but rather as buffering agents (Wang and Jaffe, 2004; Apps et al., 2010; Wilkin and DiGiulio, 2010). Instead, the release of metals from metal sulfide minerals has been explored as the primary metal source in aquifers (Zheng et al., 2009; Apps et al., 2010). While sulfide minerals are often associated with carbonate rocks and the concentration of metals in sulfides is much higher than that in carbonate minerals, sulfides in carbonate rocks generally constitute a relatively low percentage of the total rock. In addition, dissolution of carbonate minerals is more sensitive to pH variations than dissolution of sulfide minerals (Palandri and Kharaka, 2004). Thus, carbonate minerals may be a greater source of metals than associated sulfides, especially under sub-oxic conditions (Navarre-Sitchler et al., 2013). Additionally, high concentrations of Ca and Mg resulting from calcite dissolution or dolomite dissolution can outcompete trace metals in ion exchange sites and promote trace metal release into solution (Zheng et al., 2012).

Here we combine detailed characterization of two limestones, including the metal concentrations of the bulk carbonate and trace minerals and laboratory water–rock experiments with geochemical modeling to analyze the potential for metal release due to carbonate mineral dissolution in limestone aquifers and compare the metal release from carbonate dissolution and sulfide mineral dissolution.

2. Materials and methods

2.1. Rock samples

Samples were collected from well cores at the USGS Core Laboratory in Lakewood, Colorado, USA. The Joins Limestone sample came from a well drilled in Bryan Country, Oklahoma, USA (latitude/longitude 34.006996/−96.423809), at a depth of ~11,048′ below ground surface (bgs). The Kindblade Limestone sample came from a well in Carter County, Oklahoma, USA (latitude/longitude 34.330141/−97.458727), at a depth of ~10,300′ bgs. The surfaces of the rock samples were ground away to remove any contamination related to drilling, coring, storage or cutting operations. The rock samples were broken in a Rocklabs Boyd crusher and sieved to 4–30 mm in diameter. Samples for the experiments were then rinsed with Milli-Q water and dried at 50 °C for 6 h prior to storage.

2.2. Rock characterization

False color mineral maps were created for a thin section of each sample in the Advanced Mineralogy Research Center at the Colorado School of Mines, in Golden, Colorado, USA. Energy-dispersive X-ray spectroscopy (EDS) data of element distribution was collected at 10 μm spacing using a Carl Zeiss EVO 50 SEM. Quantitative evaluation of minerals by scanning electron microscopy (QEMSCAN) was used to produce mineral volume percent estimates (iDiscover software package, FEI, Inc.). The QEMSCAN analysis was not sensitive enough to determine porosity and pore surface area. Therefore, the surface area of each rock sample was determined by the BET method (with N_2 as the adsorbing gas), using a Micrometrics ASAP 2020 surface area analyzer.

The rock samples were analyzed by X-ray diffraction using a Scintag, Inc. XDS 2000. Approximately 10 g of each sample was ground in a Spex 8000 ball mill. Random orientation powders and oriented clay fractions (prepared according to the Millipore method (Moore and Reynolds, 1997)) were scanned from 4 to 50° 2-theta at a scan rate of 2° per minute and resolution of 0.02°. Mineral peaks were identified based on d-spacing versus 2-theta data from Brindley and Brown (1980) and Moore and Reynolds (1997).

Laser ablation–inductively coupled plasma-mass spectrometry (LA–ICP-MS) analysis was conducted at the Urban Environmental Biogeochemistry Laboratory at Towson University, Maryland, USA. LA–ICP-MS was performed using a CETAX LSX-213 ablation unit (213 nm Nd:YAG laser) connected to a GBC OptiMass 9500 inductively coupled plasma–time of flight–mass spectrometer with spot sizes of 150 μm for calcite and clay, and 50 μm for pyrite. The instrument was calibrated with NIST SRM glasses 610, 612 and 614, using the concentrations reported in Jochum et al. (2011). For calcite, clay (illite) and pyrite analyses, ^{44}Ca, ^{29}Si, and ^{57}Fe, respectively, were used as internal standards. Detection limits for each element were calculated as 3 σ of the background for a sample run. In the Joins Limestone, calcite ($n = 12$) and clay ($n = 12$) were each sampled 4 times in 3 different locations and seven individual pyrite grains were analyzed. In the Kindblade Limestone, only calcite was sampled ($n = 21$), as pyrite and clay could not be located with the light microscope that is integrated with the LA–ICP-MS.

Sequential metal extractions for each rock followed the method of Li et al. (1995) with minor modifications, using trace-metal grade chemicals, LC/MS-pure Optima® water (Fisher Scientific) and acid-washed supplies. In summary, the sequential extraction steps are: (1) leaching of sorbed metals, (2) dissolution of carbonate fraction, (3) dissolution of metal oxides, (4) dissolution of sulfides and organic matter, and (5) dissolution of the residual fraction from the previous steps. Modifications to the sequential extraction procedure from Li et al. (1995) were as follows: (a) the volume of 1 M sodium acetate/acetic-acid buffer in step 2 was increased to 80 ml to ensure complete dissolution of the carbonate material, and (b) in step

(5) digestion was performed using the method of Farrell et al. (1980), by which the residual fraction was dissolved in polysulfone vials, using a mixture of 1.5, 2 and 3.5 ml of reagent-grade HF, HNO_3 and HCl, respectively. Following dissolution, the HF in the mixture was neutralized by the addition of 43 ml of 1.5% H_3BO_3. Step (5) was carried out at the Laboratory for Environmental and Geological Studies, the Department of Geological Sciences, University of Colorado in Boulder, Colorado, USA. Solute concentrations of leachates from each step were analyzed using a Perkin Elmer Optima 5300 DV ICP-AES using inorganic standards "CCV-1 Solution A™" and "CCV-1 Solution B™" from High-Purity Standards, Inc. to correct for drift. A blank solution from the residual-fraction digestion was used as the background for the residual-fraction samples.

2.3. Pressurized experimental setup

In batch reactors, 150 g of each carbonate rock sample were reacted with 750 ml (water:rock ratio = 5) of 1.128 mmol/l ACS-grade NaCl solution in Milli-Q water (following Lu et al., 2010). The reactors were 1 l borosilicate glass jars sealed with Teflon-lined plastic caps and were acid-washed and heat-sterilized prior to the experiment. Each plastic cap was fitted with three 316 stainless steel bulkhead-unions. Gas flow was facilitated through 1/8″ I.D. 316 stainless steel or PFA tubing, whereas only PFA tubing was used for fluid sampling. An ISFET pH probe (Campbell Scientific, Inc.) was installed in each reactor for in-situ, continuous pH monitoring (Fig. 1). Total pressure in the reactors was maintained at 1 bar using an Equilibar QPV downstream pressure controller. A manifold was used to split the gas flow from a single tank to the headspace of each reactor (Fig. 1). The partial-pressure of CO_2 was varied by using different pre-mixed CO_2–N_2 compressed-gas tanks, ranging from 1% to 100% CO_2 (Table 1). To prevent pressure loss, input gas flow was diverted instantaneously from used to new gas tanks using a three-way valve. Tubing for aqueous samples was attached to a 0.5 μm 316 stainless steel filter (Swagelok) and a three-way valve (TWV3 in Fig. 1). The three-way valve allowed for opening of the sampling tube to the atmosphere and sampling by using the pressure difference between the enclosed reactor and the atmospheric pressure.

Table 1
Stages in the pressurized experimental work.

	Stage				
	A	B	C	D	E
Stage duration (days)	5	5	10.5	10.5	10.5
Overall pressure (bar)	Atmospheric	1	1	1	1
% CO_2	0.039	0	1	10	100
% N_2	78.084	100	99	90	0

Turned the other way, the valve allowed the compressed input gas to push water remaining in the tubing back into the reactor, eliminating the need to purge sampling lines at each sampling event. The pH probes and the pressure controller were connected to a CR-1000 datalogger (Campbell Scientific) that recorded data at 15-s intervals. Experiments were conducted at room temperature (22 °C).

An experimental control containing 3 g of >99.999% pure $CaCO_3$ powder (Sigma Aldrich, Inc.) was also performed at the same time as the water–rock experiments described above. Powdered $CaCO_3$ was used as the control to maintain pH levels similar to the other reactors. In a separate experiment, 0.1942 g of pyrite (Ward's Natural Science, Inc.) was added to the pure $CaCO_3$ and NaCl solution to test the effect of elevated pCO_2 on pyrite dissolution. The pure $CaCO_3$ standard was dissolved in HCl, and the trace element composition was measured with an ICP-MS (Varian model X), at the Laboratory for Environmental and Geological Studies, the Department of Geological Sciences, University of Colorado in Boulder, Colorado, USA.

The experiments were divided into 5 stages (A through E), during which the headspace in the reactors was filled with varying partial-pressures of CO_2 (Table 1). Stage A was used to dissolve any remaining fines from the mineral surface. At the end of stage A the fluid in the reactors was replaced. In stages C through E, pre-mixed N_2–CO_2 gas was used with 1%, 10% and 100% CO_2 resulting in 0.01, 0.1 and 1 bar pCO_2 in the reactors, respectively.

During stages C through E aqueous samples were taken at 0.5, 1, 3, 6, 12, 24, 96 and 240 h after the beginning of the stage. Samples collected for cation and trace metal analysis were acidified to

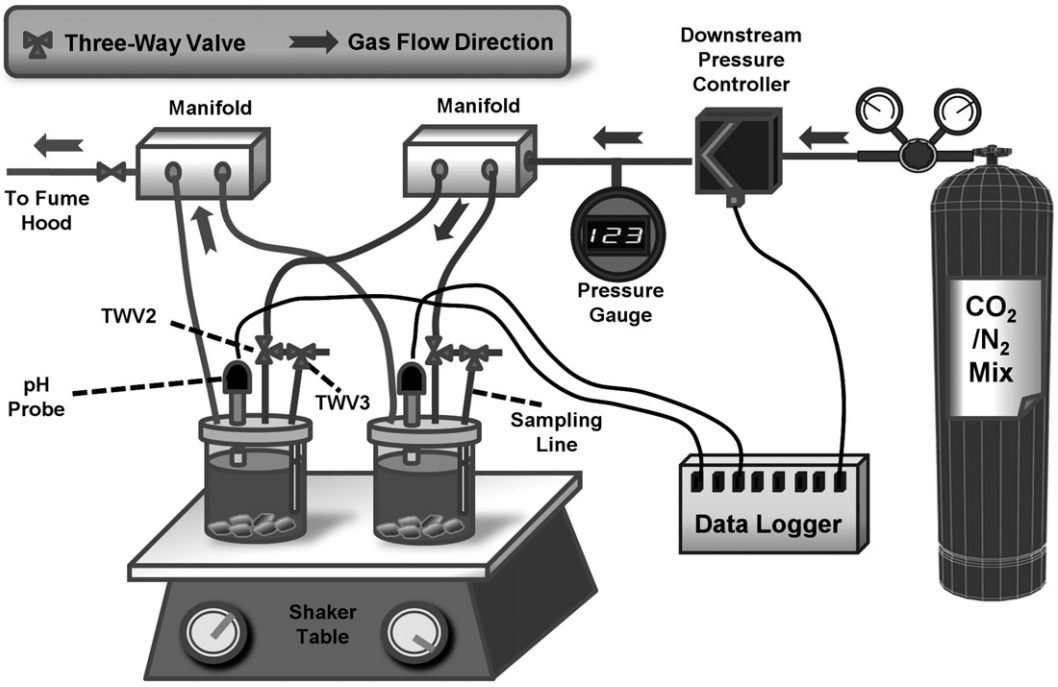

Fig. 1. Schematic diagram of the experimental setup. TWV = three-way valve.

pH < 2 with concentrated HNO_3 and analyzed with ICP-MS (Varian model X). Samples for anion analysis were not acidified, and analyzed on a liquid ion chromatograph (Dionex Series 4500I) at the Laboratory for Environmental and Geological Studies, the Department of Geological Sciences, University of Colorado in Boulder, Colorado, USA. Aqueous samples were collected from the pyrite-containing reactor with the same frequency as the other reactors, but were analyzed for sulfate only.

The approach described here allowed for the amount of dissolved CO_2 in the reactive fluid to be calculated using geochemical modeling simulations, given the pCO_2 in the headspace and measured pH (see Section 2.4). In comparison, previous experiments that focused on conditions relevant for shallow aquifers consisted mostly of bubbling CO_2 through aquifer material under atmospheric conditions (Little and Jackson, 2010; Lu et al., 2010), which provided little control on the amount of dissolved CO_2.

2.4. Geochemical modeling

Geochemical modeling was used to elucidate experimental results, and evaluate long-term metal release from carbonate aquifers. Equilibrium and kinetic geochemical simulations were performed using the geochemical code PHREEQC (Parkhurst and Appelo, 1999) and the Lawrence Livermore National Laboratory (LLNL) thermodynamic database. Additional thermodynamic constants of aqueous As–carbonate were taken from Neuberger and Helz (2005) and Sø et al. (2008). All simulations were carried out at 22 °C.

QEMSCAN mineral volumetric percents were converted to relative molar quantities in 150 g of rock and used to define the initial mineral molar quantities for geochemical simulations. In specific cases, we slightly adjusted the amounts of gypsum. The Na concentration in the simulated solutions was set to 30 mg/l, and the chloride concentration was used to maintain charge balance. The pe of the simulated solutions was set initially to 0 and allowed to vary to satisfy charge and mass balance calculations of oxygen redox pairs. Precipitation of secondary minerals was disabled in the simulations.

Kinetic calcite dissolution was calculated using the following dissolution rate (Pokrovsky et al., 2009):

$$\log R = A + B \times pCO_2 + C \times (pCO_2)^2 \quad (1)$$

where R is the dissolution rate in mol/m^2/s, and A, B and C are fitting parameters that reflect specific experimental pH and temperature. The reported values of these fitting parameters at 25 °C and pH range of 4.5–5.2 are $A = -8.69$, $B = 0.048$ and $C = 6.01 \times 10^{-4}$. Pyrite dissolution was calculated using the following dissolution rate (Palandri and Kharaka, 2004):

$$R = k_1 \times \exp\left(-\frac{Ea_1}{R_g(T-298.15)}\right) \times \left\{H^+\right\}^a \left\{Fe^{3+}\right\}^b + k_2 \times \exp\left(-\frac{Ea_2}{R_g(T-298.15)}\right) \times \left\{O_{2(aq)}\right\}^c \quad (2)$$

where k_1, k_2 (mol/m^2/s), a, b, and c (unitless) are fitting parameters, Ea is activation energy (J/mol), R_g is the gas constant (8.314 J/K/mol), and {} denotes activity of solutes. Palandri and Kharaka report fitted values to pyrite dissolution data from McKibben and Barnes (1986) of: $\log\ k_1 = -7.52$, $\log\ k_2 = -4.55$, $a = -0.5$, $b = c = 0.5$, and $Ea_1 = Ea_2 = 56.9$ J/mol. Distance from equilibrium was calculated by multiplying each rate expressions by $(1 - IAP/K)$, where IAP denotes the ion activity product and K the equilibrium constant of each mineral. Lastly, Eqs. (1) and (2) were multiplied by mineral reactive surface area to produce mass transfer rates in units of mol/s.

Assuming congruent release of impurities during mineral dissolution, the following equation was used to calculate the relative contribution of calcite dissolution and pyrite dissolution to metal concentration in solution:

$$\text{cont}_{CC/Py} = \frac{m_{CC,dis}}{m_{Py,dis}} \frac{imp_{CC}}{imp_{Py}} \quad (3)$$

where $m_{CC,dis}/m_{Py,dis}$ is the ratio of moles of dissolve calcite to moles of dissolved pyrite as calculated at each time step and cumulatively in the kinetic model, and imp_{CC}/imp_{Py} is the ratio of impurities in calcite to pyrite from the LA–ICP-MS data.

When $\text{cont}_{CC/Py} > 1$, more impurities are released to solution by calcite dissolution than by pyrite dissolution, and the opposite when $\text{cont}_{CC/Py} < 1$. This simple metric allowed us to determine which mineral is more important as a source of trace elements.

3. Results

Concentrations for all elements analyzed in the experiments are provided in electronic Appendices 1–3. Trace element concentrations reported in the results and subsequent discussion are limited to elements that were detected in the fluid during the course of the experiments and that meet the following criteria: (1) regulated in drinking waters by the United States Environmental Protection Agency (USEPA) or the State of California (Ni only) or follow release trends similar to Ca^{2+}, and (2) were not detected in the control experiments at significant concentrations.

3.1. Mineralogical composition

QEMSCAN and XRD analyses confirmed that calcite was the dominant mineral in the rocks, with minor amounts of quartz, dolomite and clay, and trace abundances of feldspar, anhydrite/gypsum, pyrite and apatite (Table 2, Fig. 2). Overall, the mineralogical distribution in the Kindblade Limestone was more homogeneous than that of the Joins Limestone.

3.2. Trace element composition of the rocks

Calcite grains were analyzed for trace metal concentrations using LA–ICP-MS in both the Kindblade and Joins samples (Table 3). In the Joins sample, single pyrite grains and clusters of clay mineral grains were analyzed with LA–ICP-MS (Table 3); in the Kindblade sample,

Table 2
Geochemical properties of the natural rock samples. Mineralogical composition is based on thin section EDS analysis (QEMSCAN).

	Joins Limestone		Kindblade Limestone	
	vol.%	Mass (mol)[a]	vol.%	Mass (mol)[a]
Quartz	7.04		3.58	
Dolomite[b]	4.68	3.9×10^{-2}	5.58	4.6×10^{-2}
Calcite	77.04	1.21[c]	89.23	1.35[c]
Calcite (Mg-bearing)[d]	1.94		1.12	
Clay	6.65[e]		0.43	
Feldspar	2.25		0.01	
Anhydrite/gypsum	0.13	9.9×10^{-4}	0.01	9.3×10^{-5}
Apatite	0.01		0.00	
Pyrite	0.20	4.6×10^{-3}	0.03	6.8×10^{-4}
Others	0.07		0.01	
BET surface area (m^2/g)	0.2883 ± 0.0018		0.1517 ± 0.0016	

[a] Mass in moles, given a total rock mass of 150 g. Molar masses are given for minerals that were included in the geochemical PHREEQC simulations.
[b] Ca-, Mg- and O-rich minerals with Ca/Mg ratios of roughly 1 to 1.47 were classified as dolomites (carbon was used to coat the carbonate samples and therefore excluded from calculations of mineral composition).
[c] Sum of "calcite" and "Mg-bearing calcite".
[d] Calcites with Ca/Mg ratios of roughly 1.48 to 27.57 were classified as "Mg-bearing calcites".
[e] Joins Limestone clays were identified as illite or glauconite with XRD.

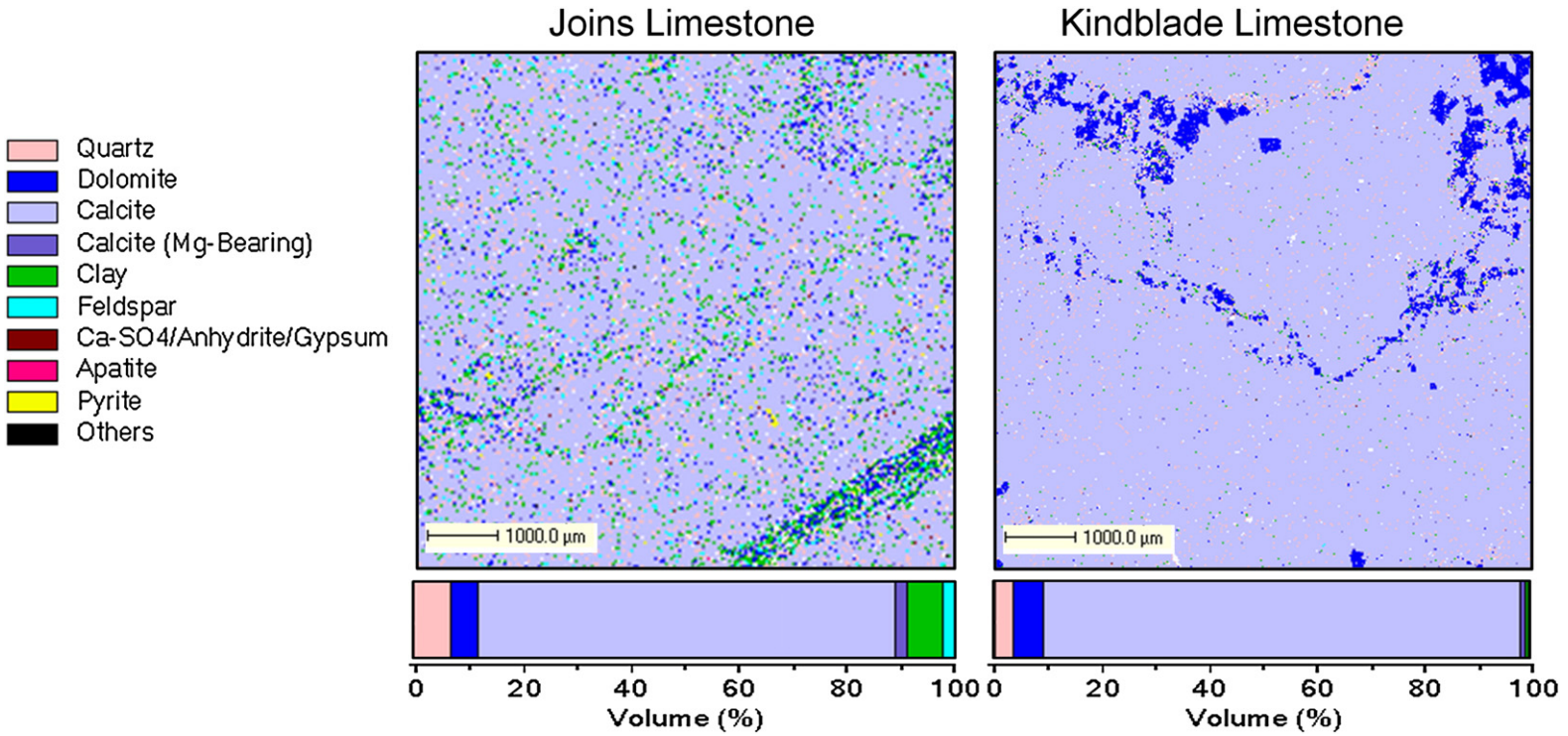

Fig. 2. Mineral abundance information and distribution maps for the Joins Limestone and the Kindblade Limestone as determined by QEMSCAN.

Table 3
Trace element composition of calcite, clay and pyrite in the studied rocks (LA–ICP-MS results), and in the pure $CaCO_3$ (complete HCl dissolution — ICP-MS results) that was used as control.

	Kindblade Limestone	Joins Limestone						Pure $CaCO_3$
	ppm[a] (n/n_{Total})[b]				Ratios			ppm
	Calcite	Calcite	Clay	Pyrite	Clay/calcite	Pyrite/calcite	Pyrite/clay	
Mg	1610 (21/21)	1004 (12/12)	2149 (12/12)	2782 (7/7)	2.14	2.77	1.29	
Co	0.6 (21/21)	1.4 (12/12)	9.7 (12/12)	91.2 (7/7)	6.88	64.86	9.43	0.5
Ni	5.8 (21/21)	5.9 (12/12)	29.5 (12/12)	296.8 (7/7)	4.97	50.06	10.06	9.5
As	<1.0 (0/21)	3.6 (10/12)	12.2 (12/12)	1449.9 (7/7)	3.37	400.97	118.83	197.7
Sr	334.8 (21/21)	503.8 (12/12)	805.5 (12/12)	199.3 (7/7)	1.6	0.4	0.25	7.4
Ba	3.5 (21/21)	37.9 (12/12)	549.9 (12/12)	723.6 (5/7)	14.5	19.08	1.32	0.3
Tl	0.1 (21/21)	0.1 (8/12)	0.8 (12/12)	6.5 (5/7)	6.99	59.83	8.56	$<2.1 \times 10^{-4}$
Pb	0.2 (21/21)	1.2 (12/12)	12.8 (12/12)	64.5 (7/7)	10.62	53.6	5.05	$<2.2 \times 10^{-5}$
U	1.0 (21/21)	0.6 (12/12)	4.1 (12/12)	<1.0 (1/7)	6.75	–	–	$<1.25 \times 10^{-5}$

[a] Average concentrations.
[b] n/n_{Total} is the number of results that were above detection limit, out of total number of measurements.

the volume fractions of pyrite and clay were low and grains were too small and dispersed to detect with the light microscope mounted in the laser ablation unit. Detection limits of trace elements in the sequential extraction analysis were generally higher than in the LA–ICP-MS analysis. As a result, several elements (Tl, U, Pb, Co) were below the detection limit in some fractions of the sequential extraction procedure, but were detected by the LA–ICP-MS (Table 3). In contrast, As was found in the carbonate fraction of the Kindblade Limestone through sequential extraction, but was not detected in the Kindblade calcite crystals using the LA–ICP-MS method (Table 3). The main results from the LA–ICP-MS analysis are:

- Concentrations of As, Ba, Ni, Tl and Pb in the Joins Limestone were higher in pyrite than those in calcite and clay on a per-mass basis (Table 3). Concentrations of Sr and U in minerals of the Joins Limestone followed the order clay > calcite > pyrite.
- Calcites in the Joins Limestone contained higher concentrations of impurities than calcites in the Kindblade Limestone, although Ni and Tl concentrations were approximately the same (Table 3).
- Sulfur was detected in significant amounts in the Joins calcite crystals (795.35 ppm on average).

The sequential extraction analysis provided insight into the concentrations of several elements of interest in different fractions of each rock (sorbed, carbonate, oxide, sulfide + organic, and residual; Fig. 3, Appendix 1). The main results from the sequential extraction analysis are:

- Several elements were more abundant in the carbonate fraction than in any other fraction in both rocks (Fig. 3, Appendix 1). These include Ba (71.1% and 80.7% of total elemental mass was found in the carbonate fractions of Kindblade and Joins, respectively), S (71.8% and 62.2%), Ni (93.4% and 60.1%), Sr (78.1% and 82.9%) and As (90.8% and 49.7%).
- The concentrations of As, Ba, Co, Ni, Pb, S and Sr in the sorbed fraction represented a small portion of the total concentration in the samples (<4%) (Fig. 3, Appendix 1). High concentrations of sorbed S (8.7% of the total) were detected in the Kindblade sample (Fig. 3, Appendix 1), yet these may be overestimates due to the presence of gypsum (see discussion in Section 4.3).
- The sulfide fraction of Joins was the main host of Co (78.7% of the total Co) and Pb (89.9% of the total Pb) in this rock, and the secondary host (after carbonate) of As (42.8% of the total As) and Ni (35.9% of the total Ni). Overall, As and Co were more abundant in the Joins Limestone than in the Kindblade Limestone (10.0 ppm compared to 3.9 ppm As, and 0.6 ppm compared to 0.07 ppm Co, respectively). The difference in As and Co concentrations between the rocks was mostly due to the presence (in Joins) or absence (in Kindblade) of sulfides. Co was below the detection limit in the carbonate fraction of both rocks (Fig. 3, Appendix 1).
- Ba concentrations were higher in Kindblade than in Joins, primarily due to the presence of Ba in the sorbed and oxide fractions (3.9% and 12.8% of total Ba concentrations, respectively) of Kindblade (Fig. 3, Appendix 1).

3.3. Pressurized dissolution experiments

At each stage of the experiment, as pCO_2 increased, the pH decreased and aqueous concentrations of many elements increased (Fig. 4, Appendix 2). All reactors showed a decrease in pH in the first 1–2 days of stages C–E (Fig. 4a), followed by a pH increase over the next 8 days. Overall, pH decreased from a value of ~9.5 in stage B to <6.5 in stage E, a trend expected from the dissolution of CO_2 in water and subsequent formation of carbonic acid. Concentrations of Ca increased at the beginning of each stage, then stabilized over the course of 10 days of reaction (Fig. 4b).

The release patterns of major, minor and trace elements into solution, as a function of pCO_2 and time, differed between metals. The main observations in the release patterns are:

- Concentrations of Ca increased at the beginning of each stage, then stabilized over the course of 10 days of reaction (Fig. 4b).
- The elements Ba (Fig. 4c), Sr (Fig. 4d), Co (Fig. 4e) and As (Fig. 4j) exhibited increases in concentration proportional to that of Ca: an initial fast release following increase in pCO_2, then approaching steady state concentrations over time. This behavior was true also for Mg in Kindblade, but not in Joins (Fig. 4f), where the release of Mg seemed to depart from the Ca trend.
- Other elements increased in concentration with increased pCO_2, but with release trends different than Ca. These include Pb (in the Kindblade reactor, Fig. 4g), Tl (Joins, Fig. 4g), Ni (Kindblade, Fig. 4h) and U (both rocks, Fig. 4i). The U, Pb and Tl concentrations

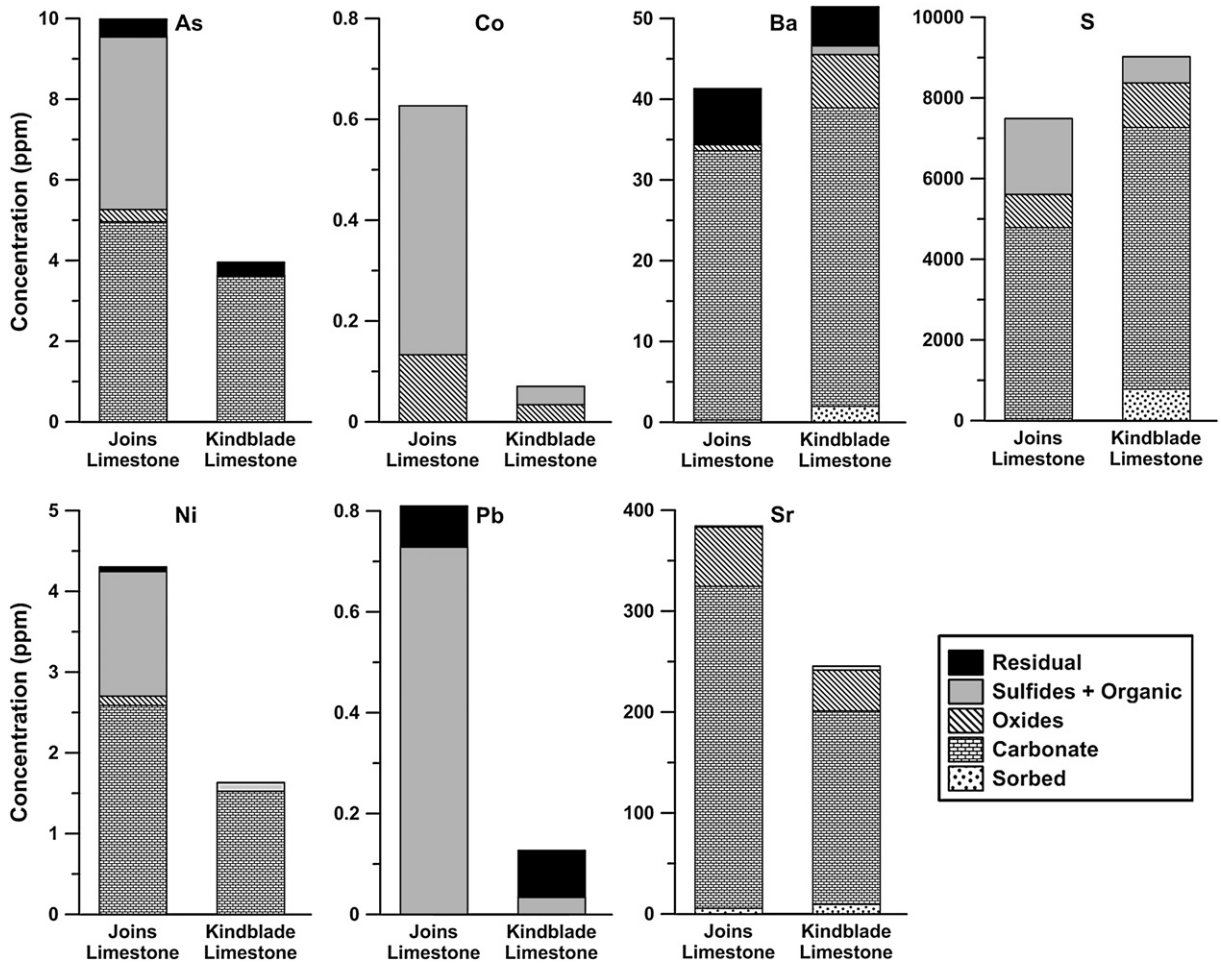

Fig. 3. Sequential extraction results for selected elements.

were <1 μg/l in all reactors. Ni spiked in the Kindblade reactor to ~870 μg/l.

- Sulfate concentrations increased throughout the experiment (Fig. 4k), although the sampling frequency and timing (3 data points overall, at the end of stages C, D and E) do not allow us to draw any conclusions regarding trends within each stage. Aqueous sulfate concentrations were lower in the Joins reactor than in the Kindblade reactor, despite higher abundances of gypsum and pyrite in the Joins Limestone (Table 2). Sulfate concentrations in the reactor containing only pyrite and pure $CaCO_3$ were very close to, or below, the detection limit of 0.2 mg/l, and comparable with the control reactor concentrations (see Appendix 3). This result strongly suggests that pyrite dissolved very slowly under our experimental conditions, and that pyrite was probably not the source of sulfate in reactors containing natural rock samples.

4. Discussion

4.1. Comparison of LA–ICP-MS and sequential extraction results

In general, sequential extraction and LA–ICP-MS indicated that the carbonate fraction of the Joins Limestone contained higher concentrations of trace metals than that of the Kindblade Limestone. For example, both methods indicated that carbonate minerals in Joins contained approximately three times more Fe and 1.5 times more Sr than the carbonate minerals in Kindblade. One exception was Ba where the LA–ICP-MS and sequential extraction results were not consistent for concentrations in carbonate minerals. Ba concentrations in the carbonate fraction of sequential extractions of both rocks were approximately the same (33.35 ppm in Joins and 36.94 ppm in Kindblade; Fig. 3). In contrast, Joins calcites contained 11 times more Ba than Kindblade calcites (37.93 ppm in Joins and 3.48 ppm in Kindblade) according to the LA–ICP-MS data (Table 3). We attribute the overestimation of Ba in the carbonate fraction and Ba in the sorbed fraction (Fig. 3) of the Kindblade to Ba-containing gypsum (Chan and Chung, 1987) that dissolved during the sequential extraction procedure but was not analyzed for by LA–ICP-MS.

4.2. Controls on release of Ca, Mg and sulfate

The distance of minerals from equilibrium is often a good indicator of the minerals that control the solubility of aqueous species (Kramer, 1967; Apps et al., 2010). Saturation indices for calcite and dolomite were <0 at the beginning of each stage and increased to saturation or near saturation at the end of each 10-day stage (Fig. 5). Gypsum and pyrite were undersaturated at the end of each stage (Fig. 5), yet for different reasons: while pyrite dissolved too slowly to reach equilibrium, reactive gypsum dissolved very quickly and was depleted before equilibrium could be achieved.

To further evaluate the extent of primary mineral dissolution in the experiments we performed equilibrium simulations of mineral dissolution at log pCO_2 ranging from −3.5 (atmospheric) to 0 with varying mineral compositions. Initial mineral quantities were based on QEMSCAN results (Table 2) and the aqueous concentrations of Ca^{2+}, Mg^{2+} and SO_4^{2-} were compared to measured concentrations after 10 days of reaction at the equivalent experimental log pCO_2. Results from these simulations indicate that aqueous concentrations of Ca^{2+}, Mg^{2+} and SO_4^{2-} are controlled by the dissolution and solubility of calcite and gypsum (Fig. 6). When only calcite was present in the model, SO_4^{2-}

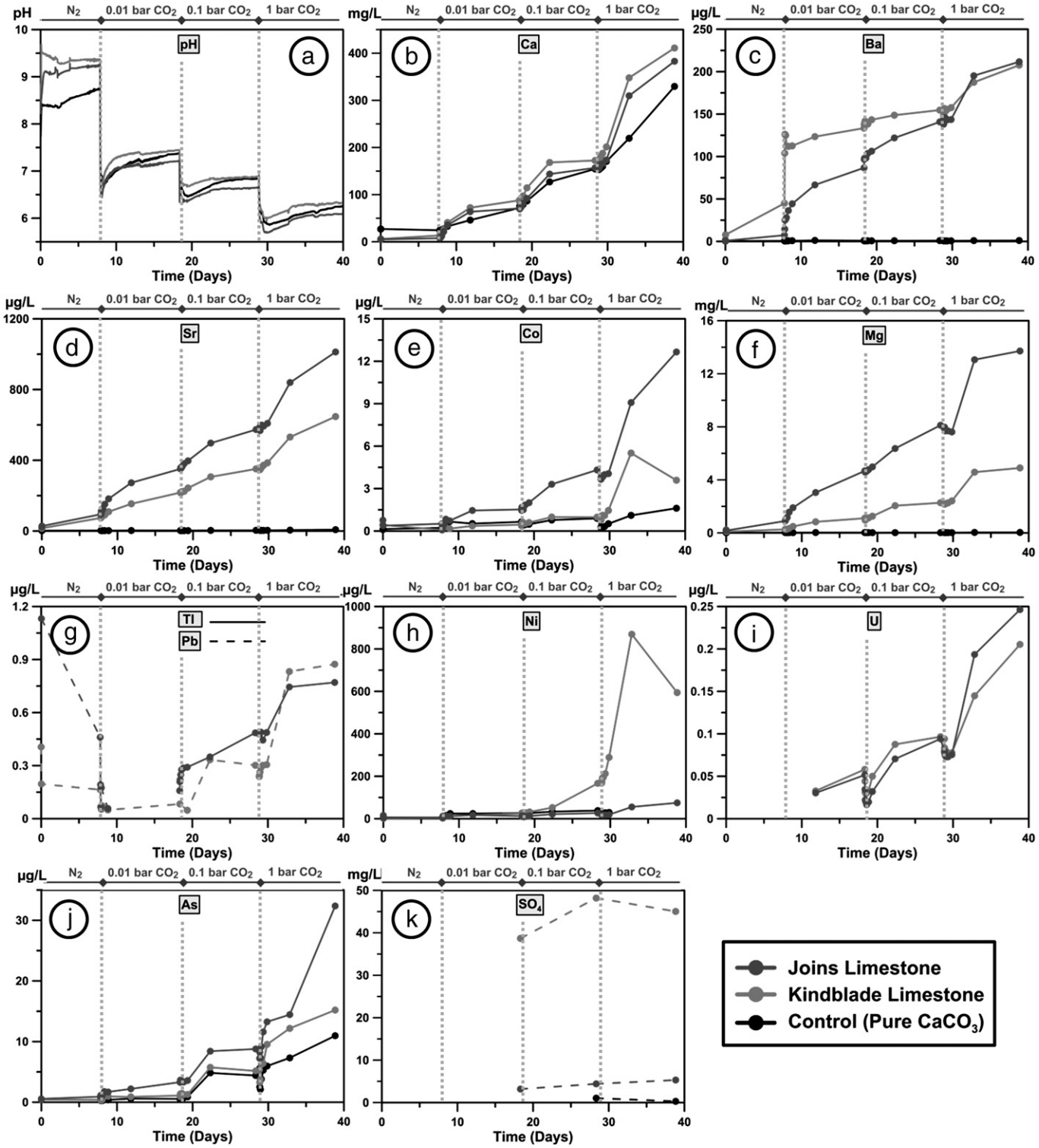

Fig. 4. Aqueous concentrations of various metals as a function of time in the pressurized experiments. Data points that were below the detection limit are not plotted (for example, Pb data from the Joins Limestone). Note that in some cases results for the control reactor overlay the x-axis, indicating that very low concentrations were detected.

concentrations were underpredicted (Fig. 6). Inclusion of pyrite in the model resulted in SO_4^{2-} concentrations much higher than observed (Fig. 6). In contrast, adding gypsum to the simulations resulted in modeled SO_4^{2-} concentrations that matched the observed, and even improved fit to Ca^{2+} observations (Fig. 6).

Similarly, when dolomite was included in the model the Mg^{2+} concentrations were higher than observed in the Kindblade reactor (Fig. 6). Dolomite was present in both rocks at approximately the same volume percent (Table 2), and calcites in the Kindblade Limestone were richer in Mg than calcites in the Joins Limestone (Table 3). However, more Mg^{2+} was released into solution in the Joins reactor than in the Kindblade reactor. Therefore, it is likely that Mg^{2+} in the Joins reactor desorbed from clays, which were present in higher abundance in the Joins Limestone compared to the Kindblade Limestone (Table 2). The

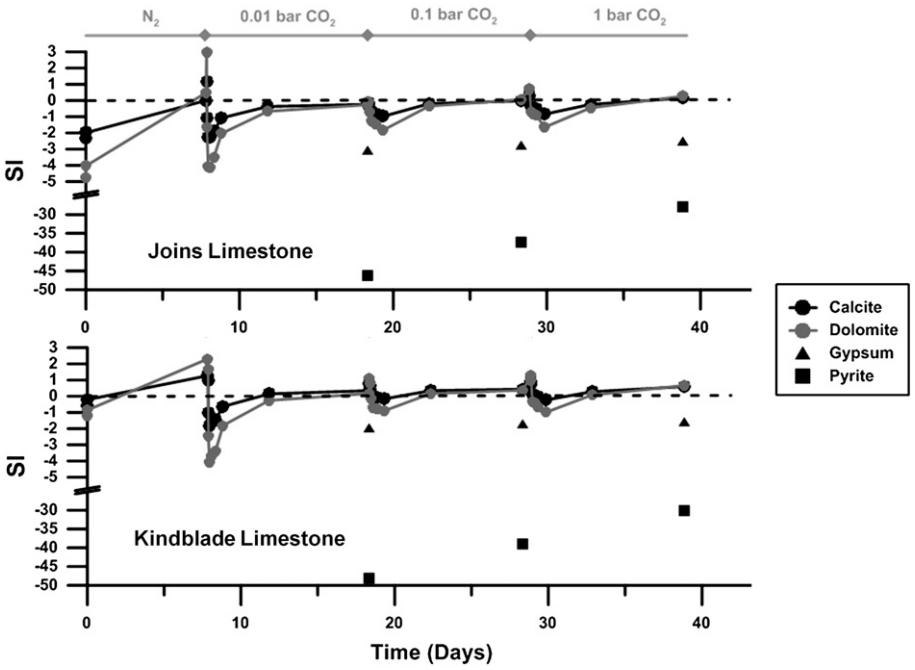

Fig. 5. Calculated saturation indices (SI) of calcite, dolomite and gypsum in the pressurized experiments. Dots indicate time intervals with calculated SI values, connecting lines were added for clarity.

lack of dolomite dissolution is consistent with previous studies demonstrating an inhibition effect of Ca^{2+} on dolomite dissolution (Busenberg and Plummer, 1982; Pokrovsky and Schott, 2001). Both experimental and modeling results suggest that calcite was the dominant carbonate mineral that dissolved in our experiment. We therefore focus on calcite, rather than dolomite, in the following discussions.

4.3. Controls of trace metal release

The relevant mechanisms controlling metal release into solution are desorption and mineral dissolution. We have established through experimental work and modeling results of major ions that calcite and gypsum were the most reactive minerals in our experiment, with calcite dissolving in the greatest quantities. However, desorption may have contributed to increased aqueous concentrations as well. In this section we compare and contrast sequential extraction, LA–ICP-MS and aqueous concentration results from the experiments to evaluate calcite dissolution and desorption as sources of trace metals to solution in the experiments.

The experimental data suggest that Sr, Co, Ba and U were released into solution through calcite dissolution. Aqueous Sr concentrations were ~1.6 times higher in the Joins reactor compared to the Kindblade reactor (Fig. 4d). Similarly, the carbonate fraction of the Joins Limestone contained 1.7 times more Sr than the carbonate fraction of the Kindblade Limestone (Appendix 1), and calcite grains in the Joins Limestone contained 1.5 times more Sr than calcite grains in the Kindblade Limestone (Table 3). We rule out desorption as the primary mechanism controlling Sr release because Kindblade contained more sorbed Sr than Joins (Appendix 1, Fig. 3), contrary to our observations of Sr in solution.

Concentrations of Co in Joins calcites were approximately 2.5 times higher than those in Kindblade calcites (Table 3), and a similar ratio was observed between aqueous Co concentrations in the Joins and Kindblade reactors (Fig. 4e). Additionally, Co concentrations in the Kindblade and control calcites were very similar (Table 3), as were the aqueous concentrations of Co in the respective reactors (Fig. 4e). Aqueous Ba and U concentrations closely followed those of Ca in both the Joins and Kindblade experiments, with the exception of a sharp increase in Ba concentration at the beginning of stage C (Fig. 4c) and decreases in U concentrations at the beginning of each stage (Fig. 4i). The sharp increase in Ba concentration is attributed to fast dissolution of gypsum (see discussion in Section 4.1). Decreased U concentrations during the first hours of each stage may be related to changes in U speciation and sorption with rapid changes in pH (Dong and Brooks, 2006).

Tl aqueous concentrations increased rapidly in the Joins reactor under 0.1 bar pCO_2 (Fig. 4g). This rapid release and the association of Tl with pyrite in the Joins Limestone, observed in X-ray adsorption spectra from scanning electron microscopy (not shown), suggest that Tl release is likely controlled by desorption from the surfaces of pyrite. The release of Tl may be enhanced by the formation of stable aqueous Tl-carbonate complexes, of which stability constants are not well constrained (Fedorenko et al., 1980; Glaser, 1995). The very low maximum contaminant level (MCL) for Tl in drinking water (0.002 mg/l; USEPA, 2011) and potential aqueous Tl-carbonate interactions make Tl an area of needed research with regard to geochemical impacts of CO_2 leakage on shallow aquifers.

Aqueous concentrations of As increased in a trend similar to Ca under 0.01 and 0.1 bar pCO_2 (Fig. 3b, j), pointing to co-dissolution with calcite (Bardelli et al., 2011; Yokoyama et al., 2012). However, As concentrations increased very quickly under pCO_2 of 1 bar, suggesting a desorption mechanism of arsenate or arsenite at this stage (Sø et al., 2008). While aqueous concentrations of As in the Joins and Kindblade reactors were comparable to the control, high concentrations of As were detected in the pure $CaCO_3$ material that was dissolved in the control reactor (Table 3).

4.4. Kinetic modeling

Calcite was close to equilibrium in our pressurized experiments within 10 days after an increase in pCO_2 (Fig. 5). Conversely, pyrite dissolution was negligible (see Appendix 3). Pyrite kinetics are very slow, driven mainly by oxidation, and to a lesser extent by an increase in acidity. While introduction of CO_2 to an aquifer system will reduce the pH and drive carbonate dissolution, it will not have a direct effect on oxygen availability, the main driver for pyrite dissolution. The question remains, whether pyrite dissolution – and release of trace metals from pyrite – is slow enough that calcite acts as the main source of metals released into solution at a time span of tens of years. We evaluate this

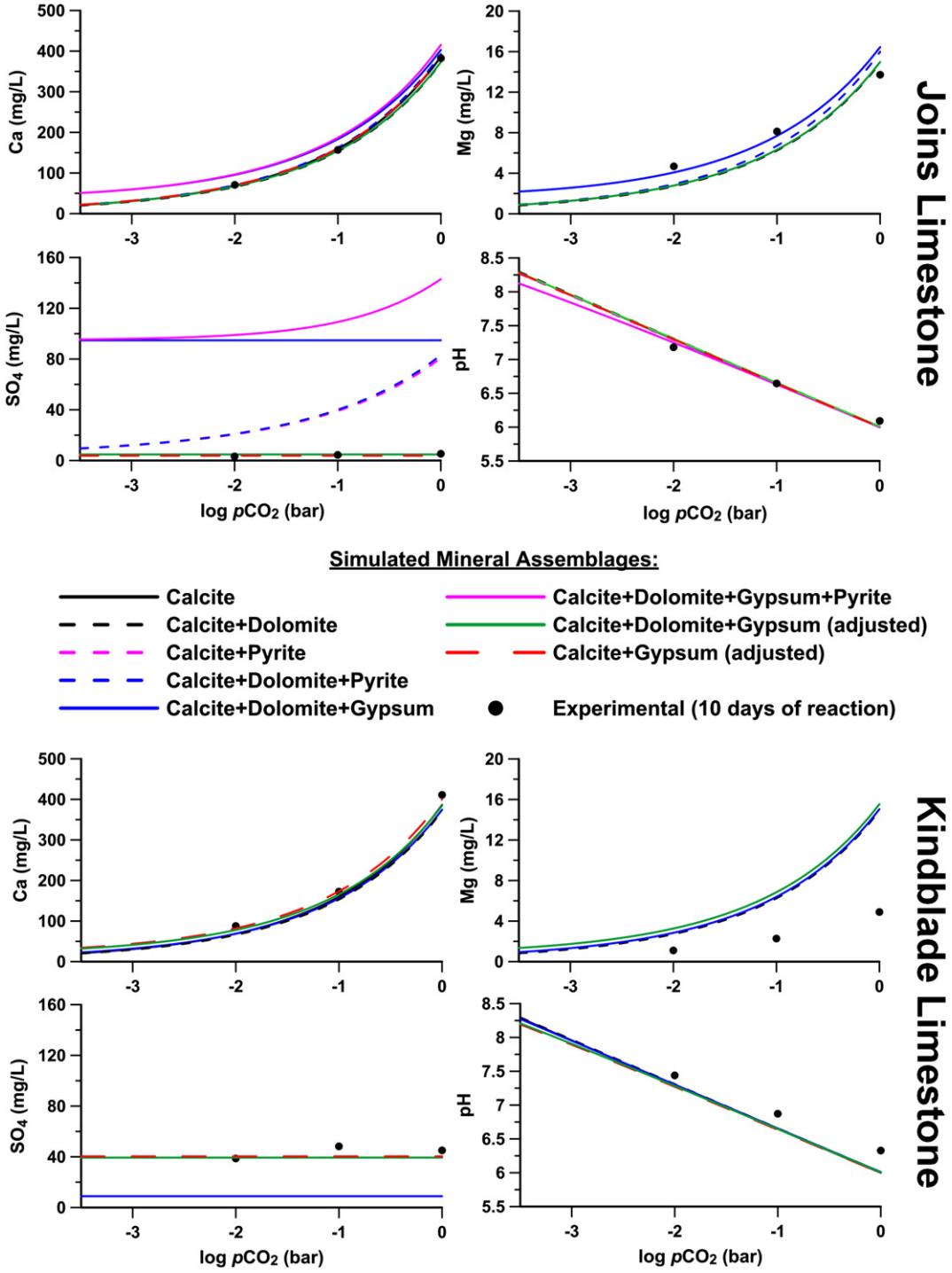

Fig. 6. Comparison of observed (experimental) and modeled concentrations in solution as a function of varying pCO_2 after 10 days of reaction. The solution chemistry of different mineral assemblages at chemical equilibrium was modeled using PHREEQC.

possibility with kinetic geochemical simulations based on our experimental results.

4.4.1. Model setup

The modeling software PHREEQC was used to simulate kinetic calcite and pyrite dissolution at elevated pCO_2 for 30 years in a batch reaction under oxidizing ($\log(pO_2) = -1$) and sub-oxic ($\log(pO_2) = -10$) conditions. These high and low pO_2 values correspond to dissolved oxygen concentrations similar to those found in principal carbonate/sandstone aquifers in the US, at the 75th and 25th percentile levels (McMahon and Chapelle, 2008). Dissolved oxygen was kept at equilibrium with the imposed pO_2. Conceptually, the oxygen boundary condition is analogous to an aquifer where water flow, and hence the rate of supply of dissolved oxygen, is faster than the rate of oxygen consumption from oxidation of sulfide and ferrous iron. Three pCO_2 boundary conditions were tested as well, in accordance with our experimental setup. The calcite dissolution rate in the model was determined by fitting the dissolution rate equation from Pokrovsky et al. (2009) (Eq. (1)) to the experimental data (Fig. 7) using a calcite surface area of 6.67 m^2 (5× less than the measured BET surface area for the rock). The pyrite dissolution rate constant was taken from Palandri and Kharaka (2004) (see Section 2.4).

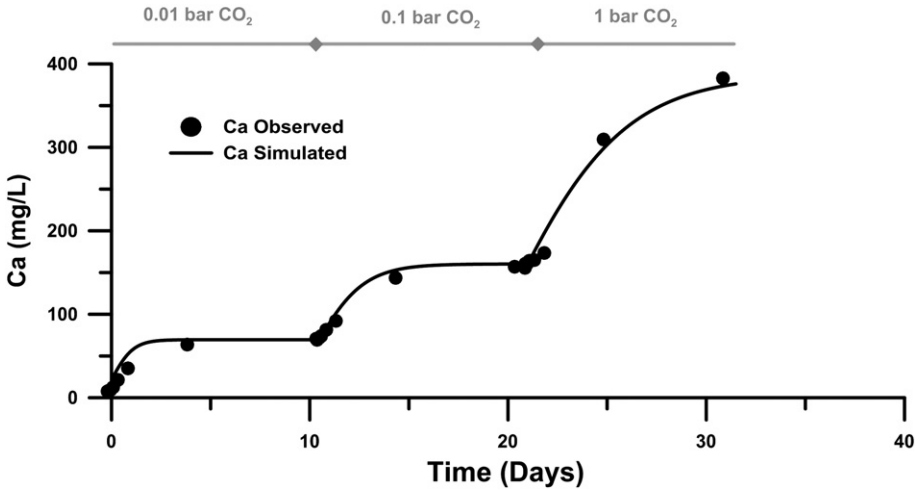

Fig. 7. Observed (experimental) Ca concentrations and simulated Ca concentrations using the formulation and parameterization of Pokrovsky et al. (2009). The total reactive surface area of calcite was adjusted from 34.95 m^2 to 6.67 m^2 to improve model fit.

A routine was created in PHREEQC to implicitly simulate pyrite crystals as surrounded by calcite in the rock matrix, in accordance with the QEMSCAN observations (Fig. 2). Thus, the modeled pyrite was not in contact with reactive fluids unless calcite dissolved. The mass of pyrite exposed to fluid resulting from calcite dissolution was calculated as follows:

$$Py(t) = Py(t-1) + Py_{\text{fresh}}(t-1) - Py_{\text{dissolved}}(t-1) \quad (4a)$$

when $Py(t-1) > Py_{\text{dissolved}}(t-1)$

$$Py(t) = Py_{\text{fresh}}(t-1) - Py_{\text{dissolved}}(t-1) \quad (4b)$$

when $Py(t-1) \leq Py_{\text{dissolved}}(t-1)$

where $Py(t)$ is the mass of pyrite that is exposed to reactions at the current time step, $Py(t-1)$ is the exposed pyrite mass from the previous time step, $Py_{\text{fresh}}(t-1)$ is the mass of pyrite newly exposed to reactions following calcite dissolution in the previous time step, and $Py_{\text{dissolved}}(t-1)$ is the mass of pyrite that is removed due to pyrite dissolution in the previous time step. At each time step, calcite dissolution was computed and the mass of calcite that dissolved was recorded. At the end of each time step, the mass of pyrite that was exposed due to calcite dissolution was assumed to be a fraction of the dissolved calcite mass (1/263, based on the molar abundance ratio of pyrite to calcite in the Joins Limestone according to the QEMSCAN analysis). The exposed pyrite mass was converted to exposed pyrite surface area by multiplying the mass by 3.01 m^2/mol (0.0251 m^2/g; McKibben and Barnes, 1986). The exposed pyrite area was then used in the next time step in conjunction with the rate expression of pyrite dissolution to determine the mass of pyrite that dissolved.

4.4.2. Modeling results

Calcite dissolution rates were higher than pyrite dissolution rates throughout the simulation in the oxic scenario, leading to higher mass of calcite dissolved compared to pyrite at every time step (Fig. 8). Calcite dissolution rates in the oxic scenario were very low after 10–30 days and both calcite and pyrite stopped dissolving at approximately 300 days as the minerals approached chemical equilibrium (Fig. 8). Pyrite dissolution in the sub-oxic scenario was initially several orders of magnitude lower than that in the oxic scenario, but the pyrite dissolution rates at later times were higher and pyrite continued to dissolve over the 30 year simulation time (Fig. 8), resulting in more pyrite dissolution in the sub-oxic scenario than in the oxic one. This result can be explained by the dependence of pyrite dissolution on calcite dissolution through exposure of pyrite surface area. In both scenarios calcite dissolution led to exposure of fresh pyrite at the beginning of the simulation (Fig. 8). Pyrite dissolution rates increased as the mass and surface area of exposed pyrite increased. Under oxic conditions, any pyrite exposed dissolved quickly due to the oxidative dissolution. After approximately 10 days the pyrite dissolution rate exceeded the exposure rate of new pyrite surfaces (Fig. 8). In contrast, under sub-oxic conditions the pyrite dissolution rate was slower than the pyrite exposure rate, and the continued pyrite dissolution fed protons to solution that continued to promote calcite dissolution and expose more pyrite (Fig. 8). Thus, the slower pyrite dissolution rate kept calcite from reaching complete equilibrium with the solution.

In both scenarios the cumulative molar mass of dissolved calcite was greater than that of pyrite (Fig. 9). Assuming stoichiometric dissolution, the ratio of Pb released into solution from calcite versus pyrite dissolution (Eq. (3)) was calculated at each time step and cumulatively. Initially, calcite was the dominant source of Pb at each time step (Fig. 10a). As calcite approached equilibrium and dissolution slowed, pyrite became the dominant source of Pb (Fig. 10a). The transition between calcite-dominated and pyrite-dominated release was between 3 and 13 days depending on the scenario. However, the cumulative release of Pb from calcite is always greater than that of pyrite in all scenarios, demonstrating the secondary role of pyrite as a source of Pb (Fig. 10b).

4.5. Implications for carbonate USDWs

The results here highlight the importance of understanding the source of metals in aquifers when using geochemical simulations to evaluate the potential for metal release in shallow aquifers impacted by a CO_2 leak. Other limestone formations will have varying concentrations of metals and varying mineralogies that will impact the magnitude of metal release from dissolution and desorption. Results of this study suggest that an evaluation of metal sources in limestone rocks (through sequential or selective extraction) can provide initial guidance regarding potential release of metals, especially if that release is expected to be controlled by calcite solubility.

Increased pCO_2 resulted in higher trace metal concentrations, and maximum concentrations were observed at 1 bar pCO_2. However, an increase in pCO_2 by an order of magnitude did not correlate to an order of magnitude increase in major and trace metal concentrations. Of the elements analyzed in the pressurized experiments, only As exceeded a federally-mandated MCL in drinking water (of 10 μg/l; USEPA, 2011) in both Kindblade and Joins reactors (Fig. 4j). Ni concentrations exceeded the State of California MCL (100 μg/l; California Code of Regulations, 2011) in the Kindblade reactor, but not in the Joins reactor (Fig. 4h). Tl concentrations exceeded the federal non-enforceable

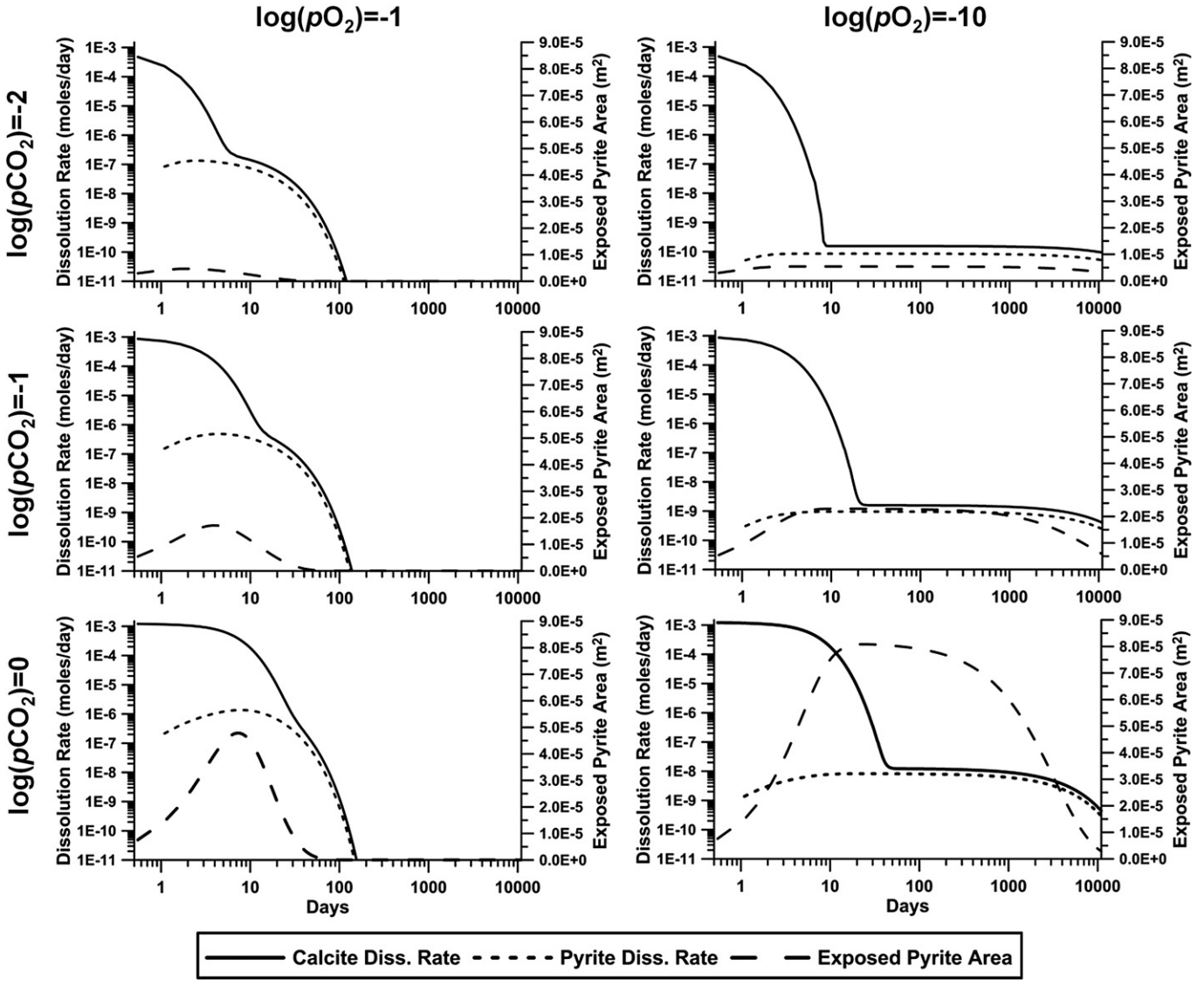

Fig. 8. Modeled calcite and pyrite dissolution rates and calculated exposed surface areas for the kinetic simulations.

maximum contaminant level goal (MCLG; 0.5 μg/l) in the Joins reactor, but remained below the MCL (of 2 μg/l) (Fig. 4g). Concentrations of U remained <1 μg/l and were far below the MCL of 30 μg/l (Fig. 4i).

While quantitative results from the batch experiments and geochemical modeling do not transfer directly to expected impacts on water quality in an aquifer setting due to high water-to-rock ratios

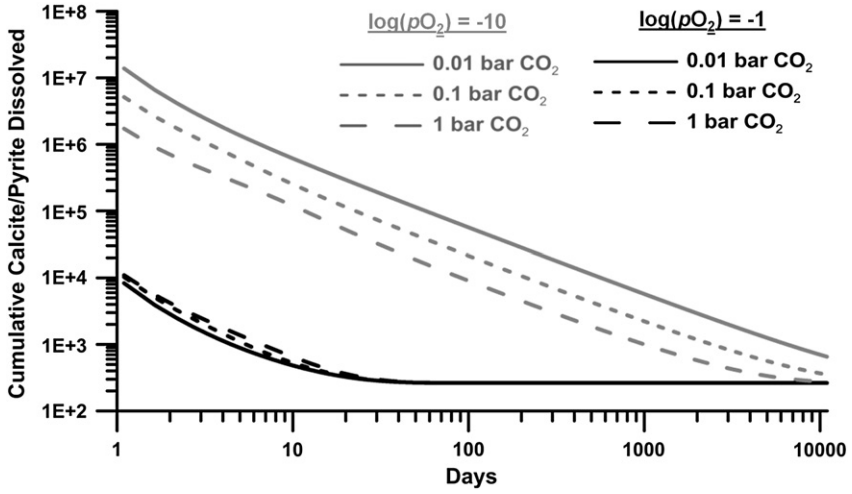

Fig. 9. Cumulative dissolution ratios of calcite and pyrite (mol calcite/mol pyrite) at various pCO_2 and various pO_2.

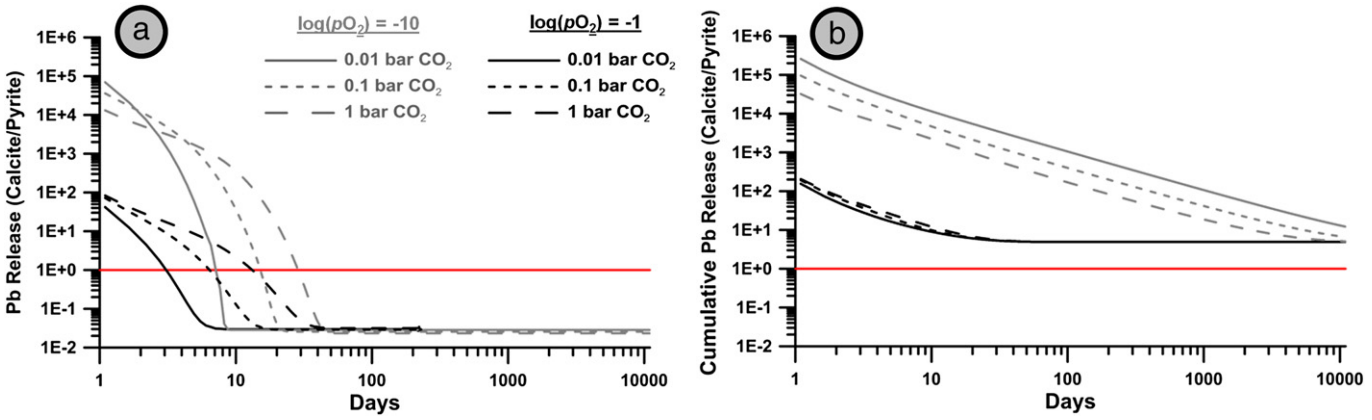

Fig. 10. Ratio of Pb release from calcite and pyrite, (a) at each time step and (b) cumulatively. The horizontal red line indicates 1:1 ratio (equal contributions of calcite and pyrite to Pb release). (For interpretation of the references to color in this figure legend, the reader is referred to the web version of this article.)

and short time scales, the results do provide insight into metals that may be released in the event of a CO_2 leak. Also, in an aquifer, solutes may be removed from solution along a flow path through sorption, precipitation and co-precipitation, regardless of their source. For example, trace elements may co-precipitate with common metal oxyhydroxides (Karthikeyan et al., 1997; Lee et al., 2002; Tokoro et al., 2010) or with calcite (Ahmed et al., 2008), although these processes were not explicitly evaluated in this study. Alternatively, some solutes may persist in solution through complexation with other solutes. In addition, the redox state, mineralogy and flow pattern in a carbonate aquifer can greatly affect the fate and transport of trace elements. The redox state of a carbonate aquifer determines the valence state of redox-sensitive aqueous species: in an oxidized carbonate aquifer, metals can precipitate as oxides, or oxy-hydroxides (Luiszer, 1987). In a reducing environment, redox-sensitive elements can remain mobilized (Oren et al., 2006). In some cases, metal mobilization may be greatest in a transition zone between oxidizing and reducing conditions (Schürch et al., 2004).

The several-order of magnitude discrepancy between mineral dissolution rates measured in a laboratory and those observed in the field has been explored in recent decades (Lichtner, 1993; White and Brantley, 2003; Navarre-Sitchler and Brantley, 2007; Li et al., 2008; Maher, 2010; Navarre-Sitchler et al., 2011; Moore et al., 2012). The factors leading to the discrepancies include differences between fresh and weathered mineral surfaces, reaction affinities, precipitation of secondary minerals, mineral age and microbial activity that sustains departure from equilibrium (Li et al., 2008 and references therein; Wallmann et al., 2008; Navarre-Sitchler et al., 2011Moore et al., 2012). Therefore, reaction rates in our simulations – originally fitted to rates observed in the laboratory – may be faster than expected in a field setting. As a result, an actual aquifer may not reach equilibrium as quickly as suggested here. From a hydrological point of view, however, our well-mixed batch kinetic model is adequate: Taylor-type dispersion (Taylor, 1953) and scale effects diminish under most natural flow velocities, and fracture flow paths longer than a few mm, for a fast-reacting mineral such as calcite (Li et al., 2008). Also, the effect of long residence time on slowing reaction rates is not pronounced when the reactions are driven by high pCO_2 (Maher, 2010).

The acute toxicity of As, and the measured aqueous concentrations relative to the USEPA-mandated MCL, warrant a further discussion on the processes that affect mobilization of As in a carbonate aquifer setting. These processes include complexation of As with carbonate ions and sorption onto calcites. Kim et al. (2000) hypothesized the persistence of stable aqueous arsenic–carbonate complexes under reducing conditions and high concentrations of carbonate ions. The stability of the aqueous complexes postulated by Kim et al. was later challenged, although an $As(OH)_2CO_3^-$ species was shown to exist with a small stability constant (Neuberger and Helz, 2005). Geochemical modeling of a system in equilibrium with calcite and at 1 bar pCO_2 shows that complexation of As with carbonate is negligible or minimal in both reducing and oxidizing conditions, even at a pCO_2 of 100 bar (Fig. 11). Therefore, As–carbonate complexation may not be an important mechanism in releasing As into the aqueous phase in carbonate aquifers at high pCO_2. When the solution is in equilibrium with calcite, the dominant species of As are either neutral (under reducing conditions; Fig. 11a) or anionic (under oxidizing conditions; Fig. 11b). The calcite surface is always positively-charged in waters containing CO_2 (Eriksson et al., 2007) and Ca > 1.6 mg/l (Foxall et al., 1979), which should promote resorption of anionic As species, and be non-reactive with respect to zero-charged As species. Indeed, adsorption and co-precipitation of As^{3+} (i.e., in reduced form) with calcite were shown to be negligible compared to adsorption and incorporation of As^{5+} (oxidized form; Sø et al., 2008; Yokoyama et al., 2012), suggesting little removal of As in reducing aquifers. Still, sorption of anionic As species on calcite will diminish in the presence of high concentrations of carbonate ions, sustaining As in solution even under oxidizing conditions (Sø et al., 2008). It is therefore imperative to focus on anion-exchange processes and aquifer redox conditions in future modeling efforts of As transport in carbonate aquifers at high pCO_2.

5. Conclusions

Laboratory experiments were used to evaluate the potential for metal release from carbonate aquifer samples under elevated pCO_2 conditions that are relevant to CO_2 leakage from geological CCUS operations. Results from these laboratory experiments were combined with detailed sample analysis to identify potential sources of metals and evaluated the relative contribution of calcite and pyrite dissolution to metal release. We find that increased pCO_2 leads to increased metal concentrations from mineral dissolution, and that calcite dissolution is the dominant mechanism of metal release. Metal desorption from mineral surfaces also contributes to some degree. Slow dissolution kinetics and low oxygen levels limited the impact of pyrite dissolution on metal release.

With the exception of arsenic and nickel, aqueous metal concentrations in the experiments did not exceed drinking-water standards. Arsenic concentrations increase above the EPA-set MCL of 10 ppb under a pCO_2 of 1 bar in both the Joins and Kindblade experiments. Nickel concentrations exceeded the State of California drinking water limit of 100 ppb under a pCO_2 of 1 bar in the Kindblade dissolution experiment. Geochemical modeling results indicate that over a 30-year time span

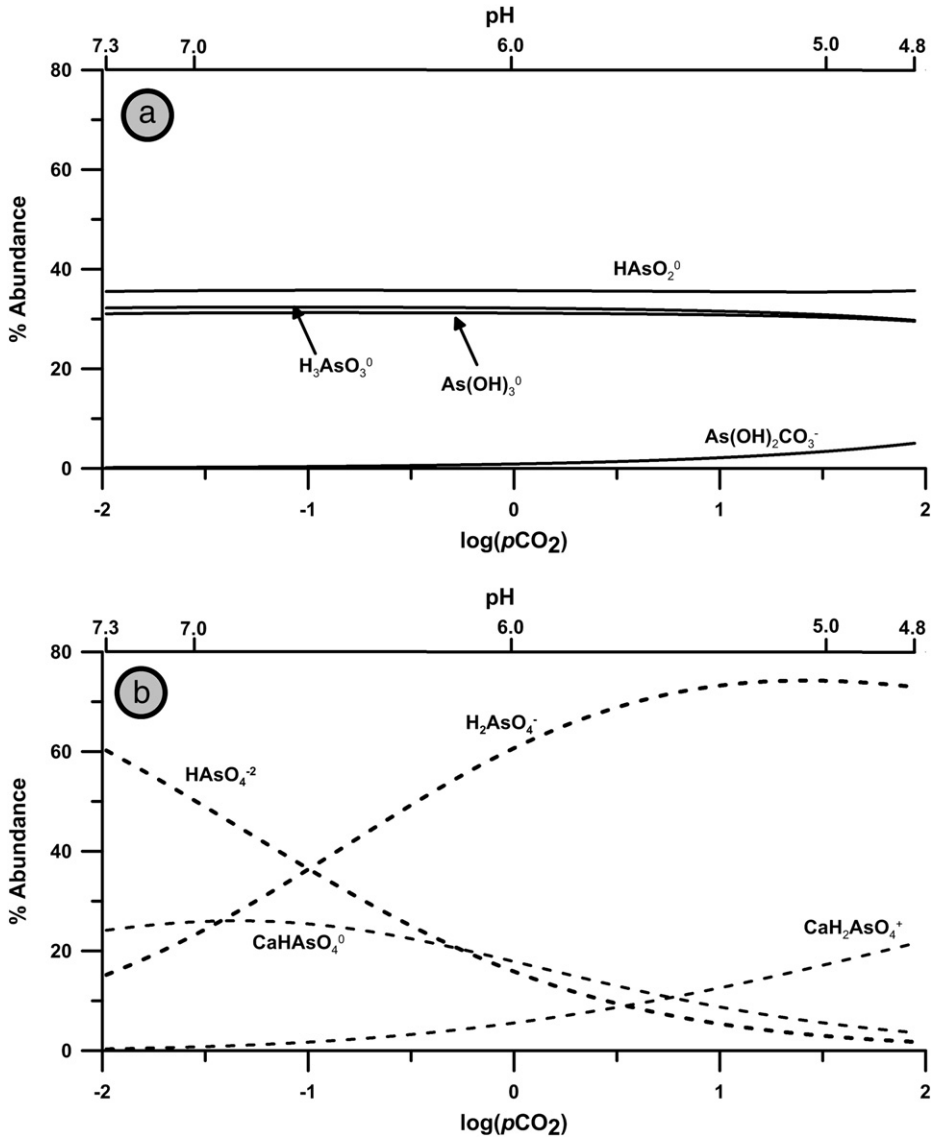

Fig. 11. Relative abundances of aqueous As species (total concentration of 20 μg/l) in a high pCO_2 system in equilibrium with calcite, under (a) reducing and (b) oxidizing conditions.

calcite dissolution will be more important to cumulative metal release in an aquifer impacted by a CO_2 leak than pyrite under either oxic or sub-oxic conditions. However, pyrite dissolution under sub-oxic conditions may play an important role in the long-term dissolution of calcite by releasing protons to solution that drive further dissolution of calcite. Where pyrite is surface-area limited – or shielded by the calcite matrix – calcite dissolution exposes the pyrite, which can then dissolve and drive further calcite dissolution in a complex feedback system. The dissolution of pyrite in our models is strongly controlled by oxygen availability under sub-oxic conditions, and by limited reactive surface area under oxidizing conditions.

This article highlights the potential impact of CO_2 leakage on carbonate aquifers, which are important sources of drinking water worldwide. We have provided evidence for calcite dissolution as an important mechanism of metal release. These results warrant further investigation of the impacts of trace metal release from carbonate minerals on water quality degradation in shallow aquifers and underground sources of drinking water in the event of a CO_2 leak. Additionally, our work highlights the importance of detailed geochemical characterization of trace metal sources, particularly in fast-dissolving mineral phases such as calcite.

Supplementary data to this article can be found online at http://dx.doi.org/10.1016/j.chemgeo.2013.10.036.

Acknowledgments

This research has been supported by a grant from the US Environmental Protection Agency's Science to Achieve Results (STAR) program. Although the research described in the article has been funded wholly or in part by the US Environmental Protection Agency's STAR program through Grant RD-83438701-0, it has not been subjected to any EPA review and therefore does not necessarily reflect the views of the Agency, and no official endorsement should be inferred. In addition, graduate student fellowship funds were donated by Information Handling Services (IHS). J.M. would like to acknowledge support of the LA–ICP-MS work by the National Science Foundation grant CHE-0959226. The authors would like to thank Katie Kirsch, Utpalendu Kuila and Matthew Dye (Colorado School of Mines), and Fred Luiszer, John Drexler and Paul Boni (University of Colorado at Boulder) for their help with various analyses and sample preparation.

References

Ahmed, I.A.M., Crout, N.M.J., Young, S.D., 2008. Kinetics of Cd sorption, desorption and fixation by calcite: a long-term radiotracer study. Geochim. Cosmochim. Acta 72 (6), 1498–1512.

Alexandratos, V.G., Elzinga, E.J., Reeder, R.J., 2007. Arsenate uptake by calcite: macroscopic and spectroscopic characterization of adsorption and incorporation mechanisms. Geochim. Cosmochim. Acta 71 (17), 4172–4187.

Apps, J.A., Zheng, L., Zhang, Y., Xu, T., Birkholzer, J.T., 2010. Evaluation of potential changes in groundwater quality in response to CO_2 leakage from deep geologic storage. Transp. Porous Media 82 (1), 215–246.

Atchley, A.L., Maxwell, R.M., Navarre-Sitchler, A.K., 2013. Using streamlines to simulate transport in CO_2-impacted drinking water aquifers. Adv. Water Resour. 52, 93–106.

Aurelio, G., et al., 2010. Structural study of selenium(IV) substitutions in calcite. Chem. Geol. 270 (1–4), 249–256.

Bardelli, F., et al., 2011. Arsenic uptake by natural calcite: an XAS study. Geochim. Cosmochim. Acta 75 (11), 3011–3023.

Bearup, L., Navarre-Sitchler, A.K., Maxwell, R.M., McCray, J.E., 2012. Kinetic metal release from competing processes in aquifers. Environ. Sci. Technol. 46 (12), 6539–6547.

Birkholzer, J.T., Zhou, Q.L., Tsang, C.F., 2009. Large-scale impact of CO_2 storage in deep saline aquifers: a sensitivity study on pressure response in stratified systems. Int. J. Greenh. Gas Control. 3 (2), 181–194.

Bogoch, R., Eldad, H., Yaacov, N., 1984. Scandium-bearing carbonates of the Tarr albitite complex, Southeast Sinai. Geochim. Cosmochim. Acta 48 (4), 885–887.

Brindley, G.W., Brown, G., 1980. Crystal structures of clay minerals and their X-ray identification. Monograph 5. Mineralogical Society, London (495 pp.).

Busenberg, E., Plummer, L.N., 1982. The kinetics of dissolution of dolomite in CO_2–H_2O systems at 1.5 °C to 65 °C and O-atm to 1-atm pCO_2. Am. J. Sci. 282 (1), 45–78.

Cahill, A.G., Jakobsen, R., Mathiesen, T.B., Jensen, C.K., 2013. Risks attributable to water quality changes in shallow potable aquifers from geological carbon sequestration leakage into sediments of variable carbonate content. Int. J. Greenh. Gas Control. 19, 117–125.

California Code of Regulations, 2011. Maximum contaminant levels — inorganic chemicals. California Code of Regulations, Title 22, Division 4, Chapter 15, Article 4, § 66431.

Chan, L.H., Chung, Y., 1987. Barium and radium in the Dead-Sea. Earth Planet. Sci. Lett. 85 (1–3), 41–53.

Comans, R.N.J., Middelburg, J.J., 1987. Sorption of trace-metals on calcite — applicability of the surface precipitation model. Geochim. Cosmochim. Acta 51 (9), 2587–2591.

Davies, W.E., Simpson, J.S., Ohlmacher, G.C., Kirk, W.S., Newton, E.G., 1984. Engineering Aspects of Karst.Department of the Interior, U.S. Geological Survey.

Dong, W.M., Brooks, S.C., 2006. Determination of the formation constants of ternary complexes of uranyl and carbonate with alkaline earth metals (Mg^{2+}, Ca^{2+}, Sr^{2+}, and Ba^{2+}) using anion exchange method. Environ. Sci. Technol. 40 (15), 4689–4695.

Duguid, A., Scherer, G.W., 2010. Degradation of oilwell cement due to exposure to carbonated brine. Int. J. Greenh. Gas Control. 4 (3), 546–560.

Elzinga, E.J., et al., 2002. EXAFS study of rare-earth element coordination in calcite. Geochim. Cosmochim. Acta 66 (16), 2875–2885.

Eriksson, R., Merta, J., Rosenholm, J.B., 2007. The calcite/water interface: I. Surface charge in indifferent electrolyte media and the influence of low-molecular-weight polyelectrolyte. J. Colloid Interface Sci. 313 (1), 184–193.

Farrell, R.F., Matthes, S.A., Mackie, A.J., United, S., 1980. A simple, low-cost method for the dissolution of metal and mineral samples in plastic pressure vessels. Report of Investigations/United States.Bureau of Mines;8480. U.S. Dept. of the Interior, Bureau of Mines, Washington, D.C.(14 pp.).

Fedorenko, A.M., Perekhod, A.F., Bobryshev, V.G., Shul'gin, V.F., 1980. Study of carbonato-complexes of thallium(I) by an interference version of the solubility method. Russ. J. Inorg. Chem. 25 (4), 931–936.

Fisler, D.K., Gale, J.D., Cygan, R.T., 2000. A shell model for the simulation of rhombohedral carbonate minerals and their point defects. Am. Mineral. 85 (1), 217–224.

Ford, D.C., Williams, P.W., 2007. Karst Hydrogeology and Geomorphology. John Wiley & Sons Ltd, West Sussex, England (562 pp.).

Foxall, T., Peterson, G.C., Rendall, H.M., Smith, A.L., 1979. Charge determination at calcium salt/aqueous solution interface. J. Chem. Soc. Faraday Trans. 1 Phys. Chem. Condens. Phs. 75, 1034–1039.

Frye, E., Bao, C., Li, L., Blumsack, S., 2012. Environmental controls of cadmium desorption during CO_2 leakage. Environ. Sci. Technol. 46 (8), 4388–4395.

Gasda, S.E., Bachu, S., Celia, M.A., 2004. Spatial characterization of the location of potentially leaky wells penetrating a deep saline aquifer in a mature sedimentary basin. Environ. Geol. 46 (6), 707–720.

Gaus, I., Azaroual, M., Czernichowski-Lauriol, I., 2005. Reactive transport modelling of the impact of CO_2 injection on the clayey cap rock at Sleipner (North Sea). Chem. Geol. 217 (3–4), 319–337.

Glaser, J., 1995. Advances in thallium aqueous solution chemistry. Adv. Inorg. Chem. 43, 1–78.

Harstad, A.O., Stipp, S.L.S., 2007. Calcite dissolution: effects of trace cations naturally present in Iceland spar calcites. Geochim. Cosmochim. Acta 71 (1), 56–70.

Harvey, O.R., et al., 2013. Geochemical implications of gas leakage associated with geologic CO_2 storage — a qualitative review. Environ. Sci. Technol. 47 (1), 23–36.

Heath, J., McPherson, B., Dewers, T., 2011. Natural Tracers and Multi-Scale Assessment of Caprock Sealing Behavior: A Case Study of the Kirtland Formation, San Juan Basin.U.S. Department of Energy.

Jochum, K.P., et al., 2011. Determination of reference values for NIST SRM 610–617 glasses following ISO guidelines. Geostand. Geoanal. Res. 35 (4), 397–429.

Karthikeyan, K.G., Elliott, H.A., Cannon, F.S., 1997. Adsorption and coprecipitation of copper with the hydrous oxides of iron and aluminum. Environ. Sci. Technol. 31 (10), 2721–2725.

Kim, M.J., Nriagu, J., Haack, S., 2000. Carbonate ions and arsenic dissolution by groundwater. Environ. Sci. Technol. 34 (15), 3094–3100.

Kramer, J.R., 1967. Equilibrium models and composition of the Great Lakes, equilibrium concepts in natural water systems. Adv. Chem. Am. Chem. Soc. 243–254.

Lee, G., Bigham, J.M., Faure, G., 2002. Removal of trace metals by coprecipitation with Fe, Al and Mn from natural waters contaminated with acid mine drainage in the Ducktown Mining District, Tennessee. Appl. Geochem. 17 (5), 569–581.

Li, X.D., Coles, B.J., Ramsey, M.H., Thornton, I., 1995. Sequential extraction of soils for multielement analysis by ICP-AES. Chem. Geol. 124 (1–2), 109–123.

Li, L., Steefel, C.I., Yang, L., 2008. Scale dependence of mineral dissolution rates within single pores and fractures. Geochim. Cosmochim. Acta 72 (2), 360–377.

Lichtner, P.C., 1993. Scaling properties of the time-space kinetic mass transport equations and the local equilibrium limit. Am. J. Sci. 293 (4), 257–296.

Lindeberg, E., 1997. Escape of CO_2 from aquifers. Energy Convers. Manag. 38 (Supplement 1), S235–S240.

Lindsey, B.D., Berndt, M.P., Katz, B.G., Ardis, A.F., Skach, K.A., 2009. Factors affecting water quality in selected carbonate aquifers in the United States, 1993–2005. US Geol. Surv. Sci. Investig. Rep. 2008–5240.

Little, M.G., Jackson, R.B., 2010. Potential impacts of leakage from deep CO_2 geosequestration on overlying freshwater aquifers. Environ. Sci. Technol. 44 (23), 9225–9232.

Lu, J.M., Partin, J.W., Hovorka, S.D., Wong, C., 2010. Potential risks to freshwater resources as a result of leakage from CO_2 geological storage: a batch-reaction experiment. Environ. Earth Sci. 60 (2), 335–348.

Luiszer, F.G., 1987. Genesis of the Cave of the Winds, Manitou Springs, Colorado. (PhD Dissertation) Department of Geological Sciences, University of Colorado, Boulder, CO (137 pp.).

Maher, K., 2010. The dependence of chemical weathering rates on fluid residence time. Earth and Planetary Science Letters 294 (1–2), 101–110.

Maupin, M.A., Barber, N.L., 2005. Estimated withdrawals from principal aquifers in the United States, 2000. U.S. Geol. Surv. Circ. 1279.

McKibben, M.A., Barnes, H.L., 1986. Oxidation of pyrite in low temperature acidic solutions: rate laws and surface textures. Geochim. Cosmochim. Acta 50 (7), 1509–1520.

McMahon, P.B., Chapelle, F.H., 2008. Redox processes and water quality of selected principal aquifer systems. Ground Water 46 (2), 259–271.

Moore, D.M., Reynolds, R.C., 1997. X-Ray Diffraction and the Identification and Analysis of Clay Minerals. Oxford University Press, Oxford, UK (378 pp.).

Moore, J., Lichtner, P.C., White, A.F., Brantley, S.L., 2012. Using a reactive transport model to elucidate differences between laboratory and field dissolution rates in regolith. Geochim. Cosmochim. Acta 93, 235–261.

Navarre-Sitchler, A.K., Brantley, S.L., 2007. Basalt weathering across scales. Earth Planet. Sci. Lett. 261 (1–2), 321–334.

Navarre-Sitchler, A.K., Steefel, C.I., Sak, P.B., Brantley, S.L., 2011. A predictive model for weathering rind formation on basalt. Geochim. Cosmochim. Acta 75, 7644–7667.

Navarre-Sitchler, A.K., Maxwell, R.M., Siirila, E.R., Hammond, G.E., Lichtner, P.C., 2013. Elucidating geochemical response of shallow heterogeneous aquifers to CO_2 leakage using high-performance computing: implications for monitoring of CO_2 sequestration. Adv. Water Resour. 53, 45–55.

Neuberger, C.S., Helz, G.R., 2005. Arsenic(III) carbonate complexing. Appl. Geochem. 20 (6), 1218–1225.

Oren, O., Gavrieli, I., Burg, A., Guttman, J., Lazar, B., 2006. Manganese mobilization and enrichment during soil aquifer treatment (SAT) of effluents, the Dan Region Sewage Reclamation Project (Shafdan), Israel. Environ. Sci. Technol. 41 (3), 766–772.

Palandri, J.L., Kharaka, Y.K., 2004. A compilation of rate parameters of water–mineral interaction kinetics for application to geochemical modeling. US Geological Survey Open File Report 2004-1068.

Parkhurst, D.L., Appelo, C.A.J., 1999. User's guide to PHREEQC (version 2): a computer program for speciation, batch reaction, one-dimensional transport, and inverse geochemical calculations. U.S. Geological Survey Water Resources Investigations 99-4259.

Pingitore, N.E., et al., 1992. Mode of incorporation of Sr^{2+} in calcite — determination by X-ray absorption-spectroscopy. Geochim. Cosmochim. Acta 56 (4), 1531–1538.

Pokrovsky, O.S., Schott, J., 2001. Kinetics and mechanism of dolomite dissolution in neutral to alkaline solutions revisited. Am. J. Sci. 301 (7), 597–626.

Pokrovsky, O.S., Golubev, S.V., Schott, J., Castillo, A., 2009. Calcite, dolomite and magnesite dissolution kinetics in aqueous solutions at acid to circumneutral pH, 25 to 150 degrees C and 1 to 55 atm pCO_2: new constraints on CO_2 sequestration in sedimentary basins. Chem. Geol. 265 (1–2), 20–32.

Reeder, R.J., Lamble, G.M., Lee, J.F., Staudt, W.J., 1994. Mechanism of SeO_4^{2-} substitution in calcite — an XAFS study. Geochim. Cosmochim. Acta 58 (24), 5639–5646.

Reeder, R.J., Lamble, G.M., Northrup, P.A., 1999. XAFS study of the coordination and local relaxation around Co^{2+}, Zn^{2+}, Pb^{2+}, and Ba^{2+} trace elements. Am. Mineral. 84 (7–8), 1049–1060.

Rouff, A.A., Elzinga, E.J., Reeder, R.J., Fisher, N.S., 2004. X-ray absorption spectroscopic evidence for the formation of Pb(II) inner-sphere adsorption complexes and precipitates at the calcite–water interface. Environ. Sci. Technol. 38 (6), 1700–1707.

Schürch, M., Edmunds, W.M., Buckley, D., 2004. Three-dimensional flow and trace metal mobility in shallow Chalk groundwater, Dorset, United Kingdom. J. Hydrol. 292 (1–4), 229–248.

Siirila, E.R., Navarre-Sitchler, A.K., Maxwell, R.M., McCray, J.E., 2012. A quantitative methodology to assess the risks to human health from CO_2 leakage into groundwater. Adv. Water Resour. 36, 146–164.

Sø, H.U., Postma, D., Jakobsen, R., Larsen, F., 2008. Sorption and desorption of arsenate and arsenite on calcite. Geochim. Cosmochim. Acta 72 (24), 5871–5884.

Sturchio, N.C., Antonio, M.R., Soderholm, L., Sutton, S.R., Brannon, J.C., 1998. Tetravalent uranium in calcite. Science 281 (5379), 971.
Tang, Y.Z., Elzinga, E.J., Lee, Y.J., Reeder, R.J., 2007. Coprecipitation of chromate with calcite: batch experiments and X-ray absorption spectroscopy. Geochim. Cosmochim. Acta 71 (6), 1480–1493.
Taylor, G., 1953. Dispersion of soluble matter in solvent flowing slowly through a tube. Proc. R. Soc. Lond. A Math. Phys. Sci. 219 (1137), 186–203.
Thorstenson, D.C., Plummer, L.N., 1977. Equilibrium criteria for two-component solids reacting with fixed composition in an aqueous phase; example, the magnesian calcites. Am. J. Sci. 277 (9), 1203–1223.
Tokoro, C., Yatsugi, Y., Koga, H., Owada, S., 2010. Sorption mechanisms of arsenate during coprecipitation with ferrihydrite in aqueous solution. Environ. Sci. Technol. 44 (2), 638–643.
USEPA, 2011. 2011 Edition of the Drinking Water Standards and Health Advisories. Office of Water, U.S. Environmental Protection Agency, Washington, DC (EPA 820-R-11-002).
Wallmann, K., et al., 2008. Silicate weathering in anoxic marine sediments. Geochim. Cosmochim. Acta 72 (12), 2895–2918.
Wang, S., Jaffe, P.R., 2004. Dissolution of a mineral phase in potable aquifers due to CO_2 releases from deep formations; effect of dissolution kinetics. Energy Convers. Manag. 45 (18–19), 2833–2848.
White, A.F., Brantley, S.L., 2003. The effect of time on the weathering of silicate minerals: why do weathering rates differ in the laboratory and field? Chem. Geol. 202 (3–4), 479–506.
Wilkin, R.T., DiGiulio, D.C., 2010. Geochemical impacts to groundwater from geologic carbon sequestration: controls on pH and inorganic carbon concentrations from reaction path and kinetic modeling. Environ. Sci. Technol. 44 (12), 4821–4827.
Wunsch, A., Navarre-Sitchler, A.K., Moore, J., Ricko, A., McCray, J.E., 2013. Metal release from dolomites at high partial-pressures of CO_2. Appl. Geochem. 38, 33–47.
Yokoyama, Y., Tanaka, K., Takahashi, Y., 2012. Differences in the immobilization of arsenite and arsenate by calcite. Geochim. Cosmochim. Acta 91, 202–219.
Zachara, J.M., Cowan, C.E., Resch, C.T., 1991. Sorption of divalent metals on calcite. Geochim. Cosmochim. Acta 55 (6), 1549–1562.
Zheng, L., Apps, J.A., Zhang, Y., Xu, T., Birkholzer, J.T., 2009. On mobilization of lead and arsenic in groundwater in response to CO_2 leakage from deep geological storage. Chem. Geol. 268 (3–4), 281–297.
Zheng, L., et al., 2012. Geochemical modeling of changes in shallow groundwater chemistry observed during the MSU-ZERT CO_2 injection experiment. Int. J. Greenh. Gas Control. 7, 202–217.